3D Quantitative Characterization of Nickel-Yttria-stabilized zirconia Solid Oxide Fuel Cell anode Microstructure in Discharge

Zhenjun Jiao, Naoki Shikazono, Nobuhide Kasagi

Institute of Industrial Science, University of Tokyo 4-6-1, Komaba, Meguro-ku, T okyo. 153-8505, Japan

The anode microstructural evolution is correlated to its electrochemical characteristics during a long time discharge for conventional nickel-yttria-stabilized zirconia composite anode. Self made anode performance degraded with operation time in humidified hydrogen, with the increases of both ohmic and polarization losses. The anode samples after different discharging times were analysized by 3-dimensional microstructure reconstruction based on focused ion beam-scanning electron microscopy technique. Nickel connectivity, nickel-yttria-stabilized zirconia interface area and the active three-phases-boundary length were correlated to the anode degradation. The influences of bulk gas humidity and current density were also investigated to reveal their contributions to the anode degradation.

Introduction

As a high energy efficiency power generation system, solid oxide fuel cell (SOFC, hereafter) has been attracting more and more attentions in the last few decades [1]. The SOFC anode degradation mechanism has been intensively investigated, in order to achieve the actual industrial applications requirement, a durability of more than 40,000 hours. Most of the current SOFC anodes exhibit significant degradation in a long time discharge experiments, which is mainly caused by the coarsening of Ni phase, especially during the initial operation period (< 200 hours) which is associated with the initial fast growth kinetics of Ni [2-11]. The Ni coarsening effect leads to a the reduction of Ni surface (including interface) area, and a loss of Ni network connectivity as well as the active three phases boundary (TPB, hereafter) length. Furthermore, higher humidity or current density also lead to rapid anode degradation or even sudden failure [6]. Recently, 3-dimensional (3D, hereafter) reconstructions of SOFC electrode has been achieved by applying focused ion beam-scanning electron microscopy (FIB-SEM) technique [12-16]. This method provides quantitative information of composite cermet microstructure in 3D, which can be correlated to the electrode performance via phase volumetric connectivity, specific surface and interface areas and the volumetric active three-phase boundary density. In this paper, FIB-SEM 3D reconstruction technique is applied for quantitative characterization of microstructural evolution of Ni-YSZ composite anode in the initial 250 hours, which was then correlated to the initial anode performance degradation.

Experimental

The details of SOFCs fabrication process and the cell performance measurement setup has been described in Ref. [17]. The anode samples after experiments were observed by FIB-SEM (Carl Zeiss, NVision 40). The samples were first infiltrated by low viscosity epoxy resin under low pressure atmosphere (ca. 15 Pa), so that the pores of the porous electrode could be easily distinguished during FIB-SEM observation. The cured samples were then polished by using Ar-ion beam cross-section polisher (JEOL Ltd., SM-09010) for the FIB-SEM observation. The details of dual-beam FIB-SEM observation technique has been introduced in Refs. [12, 15]. The 3D microstructure of the Ni–YSZ anode was then virtually reconstructed based on a series of 2D images by Matlab and Avizo Fire 6.0 (Maxnet). The difference in contrast of FESEM images was used to distinguish the three phases of Ni, YSZ, and pore. After reconstruction, the volume fraction, phase connectivity, the ratios of surface and interface areas to total volume of each phase, and the TPB density were measured. The length of TPB was estimated by the volume expansion method in Refs. [13, 15].

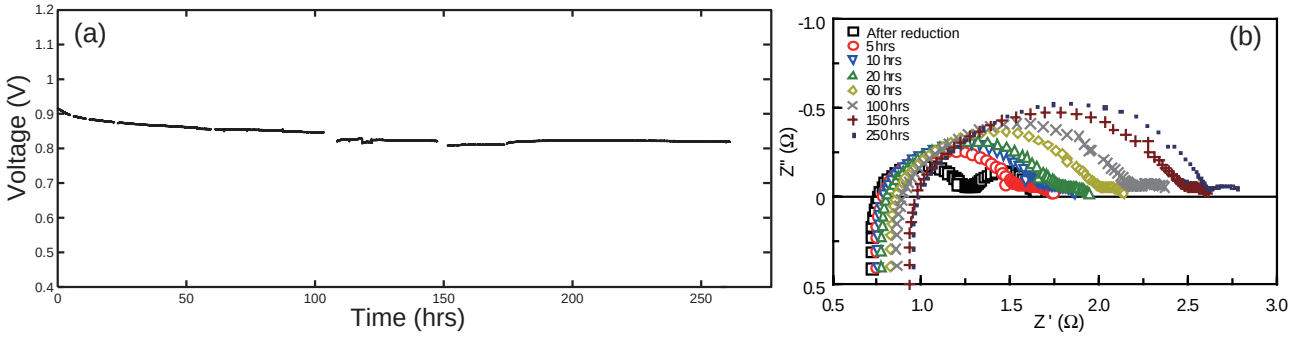

Figure.1 (a) A-R terminal voltage against time measured in 3% H2O hydrogen by galvanostatic method for 250 hours. (b) Corresponding A-R impedance spectrum (in OCV) evolution after different discharge time.

Results and Discussion

The anode was discharged in 3%H_2O humidified hydrogen with a current density of 200 $mAcm^{-2}$ for 250 hours to investigate the initial degradation of anode in standard SOFC anode operation condition. Figure 1 (a) shows the A-R terminal voltage change against time. It can be observed that after a relative fast degradation in the initial 50 hours, the anode performance maintained a relatively stable stage until the end. The A-R impedance spectrum at different time are shown in Fig. 1(b). It is seen that the A-R ohmic resistance and polarization both increased with time compared to the initial A-R impedance spectrum right after initial reduction. The ohmic losses were derived from the intersections of the impedance spectrum arc at high frequency with real axis and the polarization resistances were derived from the spanning length of the impedance arcs. During the test, the ohmic resistance increased from about 0.75 Ω to 0.98 Ω , while the polarization resistance increased from 0.54 Ω to 1.82 Ω . In the initial 100 hours, the ohmic resistance increased from 0.75 Ω to 0.97 Ω while in the last 150 hours it increased only 0.01 Ω . It can be seen that the degradation rate of ohmic resistance was initially very fast. For both ohmic resistance and polarization impedance, most of the increase was observed in the initial 100 hours.

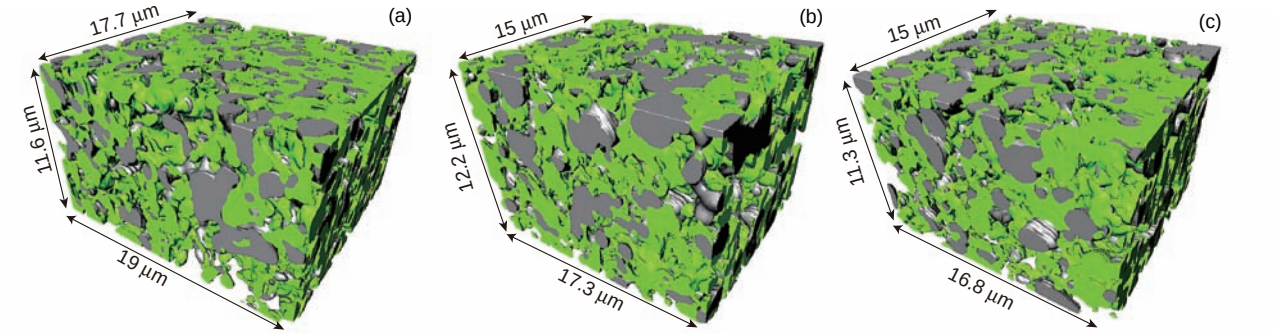

Figure 2. 3D reconstruction images of anodes (a) after reduction, after (b) 100 and (c) 250 hours discharge with a current density of 0.2 Acm−2. Gray: Ni and green: YSZ.

The 3D images of Ni-YSZ anodes were reconstructed as shown in Fig. 2. The Ni and YSZ phases are demonstrated as grey and green respectively. In Fig. 3, Ni, YSZ phase and TPB networks are shown. The red particles in Fig. 3 indicate isolated particles from the main networks which connect to the six volumetric boundary faces. The yellow particles indicate the phase portion only connected to volumetric boundary faces. It can be observed that the percolation connectivity of Ni phase deteriorates obviously with discharge time, while there is almost no change for YSZ phase. TheTPB density decreased with discharge time.

The volume fraction, percolation fraction, surface area and inter-phases surface area and the TPB networks are summarized in Table 1. The Ni-YSZ volume ratios measured were almost constant for the three samples, which validates the reconstruction process. The YSZ and pore phases both show very high percolation fractions. For Ni phase, it is clearly seen that its percolation connectivity decreases with discharge time for about 40% in 250 hours. More isolated and unknown Ni particles were formed in the discharging process. The specific surface area of Ni decreased by about 16.9% and 17.9% after 100 and 250 hours, which supports the mechanism of Ni coarsening. The percolation connectivity and specific surface area of YSZ changed slightly after discharge, which means that the YSZ particles remained undeformed with time. Ni-YSZ and Ni-Pore specific inter-phases surface area also reduced with time, while YSZ-Pore specific inter-phases surface remained unchanged. The specific TPB density reduced about 20% and 22 % after 100 and 250 hours, respectively. The decrease of both Ni surface area and Ni-YSZ inter-phases surface area may explain the decrease of total TPB density. With the reduction of Ni network percolation connectivity, the final active TPB density decreases by about 31% and 57% after 100 and 250 hours discharge, respectively.

It is well known that TPB and Ni network connectivity in Ni-YSZ composite cermet anode strongly affect its electrical performance. The anode polarization impedance and electrode-electrolyte interface ohmic resistance both depend on the anode microstructural morphology [19-21]. In this study, the reduction of both Ni network connectivity and the active TPB may explain the obvious increase of the polarization impedance shown in Fig. 1(b). The degradation rate of polarization impedance corresponds to the reduction of active TPB density, especially in the initial 100 hours. It is known that the ohmic resistance of electrolyte-support SOFC is dominated by the thick electrolyte. As reported, the ionic conductivity of 8 mol% YSZ at 800°C is 0.02 Scm^{-1}, with considering the grain boundary effect [21]. In this study, the total ohmic resistance of the

YSZ pellet is about 0.8 Ω. By using a central position reference electrode, the anode side ohmic resistance of the electrolyte is approximated to be 0.4 Ω. The extra 0.35 Ω anode ohmic resistance might be attributed to the Ni-YSZ contact ohmic resistance, which can be influenced by Ni phase microstructural change.

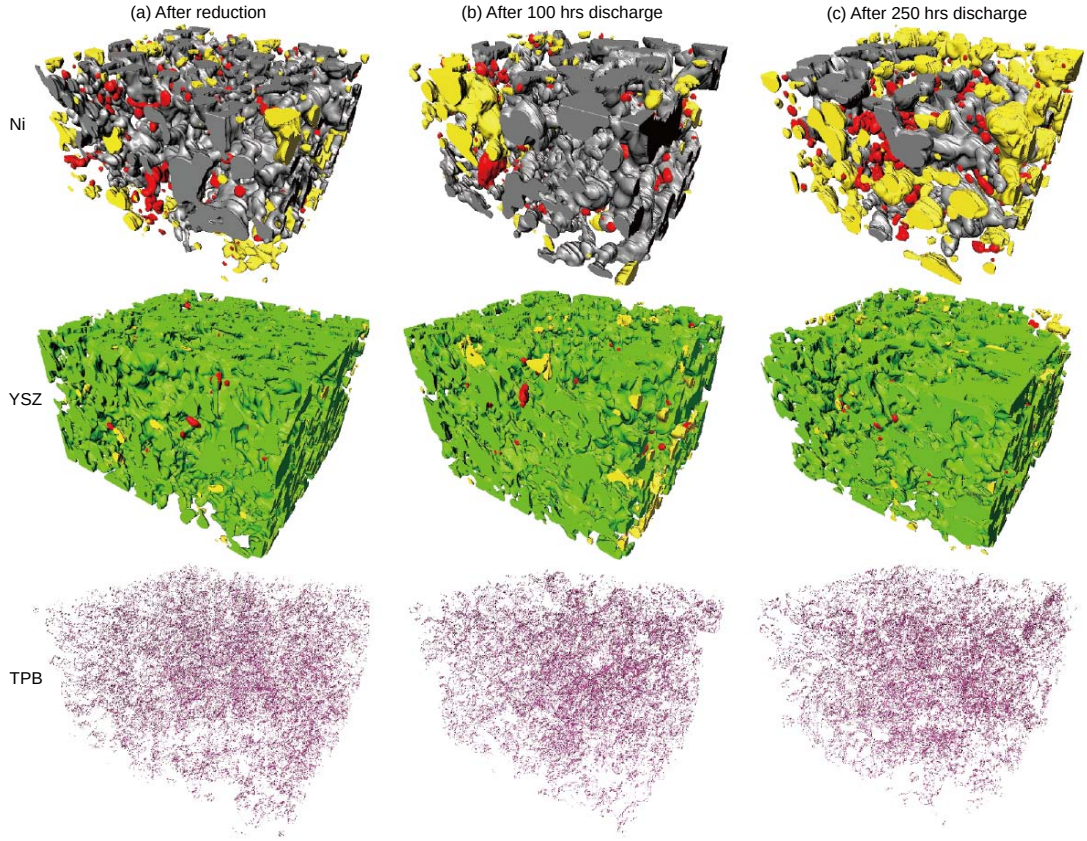

Figure 3. Separated Ni, YSZ and TPB networks corresponding to Fig. 2 (a)-(c). Red: non-percolated particle, yellow: unknown-status particle.

Table 1. Volume fraction, percolation connectivity, surface area of three phases, inter-phases contacting surface area and TPB density for the NiYSZ anode after different discharge time.

Parameter	Phase	After reduction	100 hrs discharge	250 hrs discharge
Volume fraction (%)	Ni	22.23	23.95	20.75
	YSZ	35.41	33.55	33.31
	Pore	42.36	42.5	45.94
Percolated phase fraction (%)	Ni	87.75	79.5	52.41
	YSZ	99.08	98.34	98.75
	Pore	99.72	99.82	99.82
Unknown phase fraction (%)	Ni	6.75	15.72	34.37
Isolated phase fraction (%)	Ni	5.5	4.78	13.22
Specific surface area ($\mu m^2/\mu m^3$)	Ni	0.52	0.44	0.42
	YSZ	1.01	0.96	0.96
	Pore	0.95	0.89	0.92
Specific inter-phases surface area ($\mu m^2/\mu m^3$)	Ni-YSZ	0.29	0.25	0.23
	Ni-Pore	0.23	0.18	0.19
	YSZ-Pore	0.73	0.71	0.72
TPB density ($\mu m/\mu m^3$)	Total	1.29	1.02	0.98

Conclusion

The initial fast degradation phenomena of SOFC anode performance was quantitatively investigated by FIB-SEM 3D reconstruction method. The degradation of the anode was attributed to the increase of both anode-reference polarization impedance and ohmic resistance. The increase of polarization impedance is dominated by Ni phase morphological change caused by Ni coarsening effect, which leads to continuous increase of isolated Ni particle and the loss of active TPB density.

Acknowledgments

This work was supported by the New Energy and Industrial Technology Development Organization (NEDO) under the Development of System and Elemental Technology on Solid Oxide Fuel Cell (SOFC) Project.

Reference

1. C. S. Subhash and K. Kevin, High Temperature Solid Oxide Fuel Cells: Fundamentals, Design and Applications, Elsevier Advanced Technology, (2003).
2. L. Holzer, B. Munch, B. Iwanschitz, M. Cantoni, T. Hocker and T. Graule, J. Power Sources, 196, 7076-7089 (2011). 8
3. H-Y. Chen, H-C. Yu, J. S. Cronin, J. R. Wilson, S. A. Barnett and K. Thornton, J. Power Sources, 196, 1333–1337 (2011).
4. S. P. S. Badwal and M. J. Bannister and R. H. J. Hannink, Science and Technology of Zirconia V, Technomic publishing Company, (2003).
5. S. Koch and P. V. Hendriksen, M. Mogensen, Y-L. Liu, N. Dekker, B. Rietveld, B. De. Haart and F. Tietz, Fuel Cells, 2, 130–136 (2006).
6. T. Matsui, R. Kishida, J-Y. Kim, H. Muroyama and K. Eguchi, J. Electrochem. Soc., 2, 130–136 (2010).
7. B. de Boer, Ph.D. Thesis, University of Twente, the Netherlands, (1998).
8. J. Mizusaki, H. Tagawa, T. Saito, T. Yamamura, K. Kamitani, K. Hirano, S. Ehara, T. Takagi, T. Hikita, M. Ippommatsu, S. Nakagawa and K. Hashimoto, Solid State Ionics, 70-71, 52-58 (1994).
9. J. Mizusaki, H. Tagawa, T. Saito, T. Yamamura, K. Kamitani, K. Hirano, S. Ehara, T. Takagi, T. Hikita, M. Ippommatsu, S. Nakagawa and K. Hashimoto, J. Electrochem. Soc., 141, 2129-2134 (1994).
10. M. S. Schmidt, K. V. Hansen, K. Norrman and M. Mogensen, Solid State Ionics, 180, 431-438 (2009).
11. D. Simwonis and F. Tietz and D. Stover, Solid State Ionics, 132, 241–251 (2000).
12. Z. Jiao, N. Shikazono and N. Kasagi, J. Power Sources, 24, 8019-8027 (2010).
13. H. Sumi, Kishida, J-Y. Kim, H. Muroyama, T. Matsui and K. Eguchi, J. Electrochem. Soc., 157, B1747–B1752 (2009).
14. N.Vivet,S.Chupin,E.Estrade,T.Piquero,P.L.Pommier,D.RochaisandE.Bruneton,J.PowerSources,196,7541–7549 (2011).
15. H. Iwai, N. Shikazono, T. Matsui, H. Teshima, M. Kishimoto, R. Kishida, D. Hayashi, K. Matsuzaki, D. Kanno, M. Saito, H. Muroyama, K. Eguchi, N. Kasagi and H. Yoshida, J. Power Sources, 195, 955-961 (2010)
16. T. Matsui, R. Kishida, J-Y. Kim, H. Muroyama and K. Eguchi, J. Electrochem. Soc., 157, B776–B781, (2010).
17. Z. Jiao, N. Takagi, N. Shikazono and N. Kasagi, J. Power Sources, 196, 1019-1029 (2010).
18. X. Guo, W. Sigle, J. Fleig and J. Maier, Solid State Ionics, 154-155, 555-561 (2002).
19. T. Fukui, S. Ohara, M. Naito and K. Nogi, J. Power Sources, 110, 91-95 (2002),
20. T. Fukui, S. Ohara and K. Nogi, Electrochem. Solid St., 1, 120-122 (1998).
21. K. Thyden, Ph.D. Thesis, Ris National Laboratory for Sustainable Energy, Technical University of Denmark, Denmark., (2008).